New Nanocomposite Materials with Improved Mechanical Strength and Tailored Coefficient of Thermal Expansion for Electro-Packaging Applications

metals

MDPI

Article

New Nanocomposite Materials with Improved Mechanical Strength and Tailored Coefficient of Thermal Expansion for Electro-Packaging Applications

Abdollah Saboori [1,*], Seyed Kiomars Moheimani [2], Matteo Pavese [1], Claudio Badini [1] and Paolo Fino [1]

[1] Department of Applied Science and Technology, Politecnico Di Torino, Corso Duca Degli Abruzzi 24, 10129 Torino, Italy; matteo.pavese@polito.it (M.P.); claudio.badini@polito.it (C.B.); paolo.fino@polito.it (P.F.)

[2] Department of Materials Engineering, Najafabad Branch, Islamic Azad University, Najafabad 8514143131, Iran; kiomars.moheimani@gmail.com

* Correspondence: abdollah.saboori@polito.it; Tel.: +39-011-090-4762

Received: 31 October 2017; Accepted: 28 November 2017; Published: 1 December 2017

Abstract: In this research, copper nanocomposites reinforced by graphene nanoplatelets (GNPs) were fabricated using a wet mixing method followed by a classical powder metallurgy route. In order to find the best dispersion technique, ball milling and wet mixing were chosen. Qualitative evaluation of the structure of the graphene after mixing indicated that the wet mixing is an appropriate technique to disperse the GNPs. Thereafter, the influence of graphene content on microstructure, density, hardness, elastic modulus, and thermal expansion coefficient of composites was investigated. It was shown that by increasing the graphene content the aggregation of graphene is more obvious and, thus, these agglomerates affect the final properties adversely. In comparison with the unreinforced Cu, Cu–GNP composites were lighter, and their hardness and Young's modulus were higher as a consequence of graphene addition. According to the microstructural observation of pure copper and its composites after sintering, it was concluded that grain refinement is the main mechanism of strengthening in this research. Apart from the mechanical characteristics, the coefficient of thermal expansion of composites decreased remarkably and the combination of this feature with appropriate mechanical properties can make them a promising candidate for use in electronic packaging applications.

Keywords: metal matrix nanocomposite; copper; graphene; dispersion; powder metallurgy; thermal expansion coefficient; thermal conductivity; electrical resistance

1. Introduction

Nowadays, Metal Matrix Nanocomposites (MMNCs) are materials which are used extensively in different applications such as automotive, aerospace, and electronic packaging industries [1–4]. For instance, consider the field of electronic packaging: with the progress of technology and the corresponding increase in the performance of electronic devices, the devices release more heat, and thermal considerations in the design and material selection thus become seriously important factors [5]. Indeed, the functioning and useful life of packaged electronic assembly depend seriously on advanced electronic packaging materials. Electrical conduction, electrical insulation, mechanical support, environmental protection, and thermal conduction and dissipation are the main functions that should be considered [6,7]. Heat sinks, which are the cooling systems for electronic devices, have been developed to solve this issue. It has been indicated that materials with a thermal conductivity higher than 150 W/(m·K) and coefficient of thermal expansion (CTE) between 4×10^{-6} K^{-1} and 9×10^{-6} K^{-1} are desirable materials for use in this application [8].

To select a proper material to be employed in electronic packaging applications, different considerations should be taken into account to strike a balance between function, performance, manufacturability, reliability, and cost [9]. Among the metallic materials, copper is one of the most interesting candidates which can be used in electronic packaging applications, owing mainly to its high thermal conductivity and cost. However, its high thermal expansion coefficient (16.9×10^{-6} K^{-1}) at ambient temperature and low tensile strength have limited its application. Thus, in order to address these drawbacks and broaden the application of copper and its alloys, it is necessary to improve these characteristics through either fabrication of composites or heat treatment. However, in order to develop the application of copper composites, it is necessary to fabricate new composites with high thermal and electrical conductivity, low coefficient of thermal expansion, and high mechanical properties. Thus, it is essential to design the material to have a uniform dispersion of reinforcing material as well as a strong interfacial bonding between the reinforcement and matrix. Generally speaking, copper matrix composites can be produced by the addition of stable and non-soluble particles into the copper matrix. These non-soluble and stable particles can be different based on the target application, and could be oxides (Al_2O_3, SiO_2, etc.), borides (TiB_2, ZrB_2, etc.), nitrides (TiN, ZrN, etc.), carbides (SiC, B_4C, TiC, etc.), or carbonaceous materials (CNTs, graphite, graphene, diamond) [10–12]. According to the literature, due to the poor wettability between molten copper and reinforcing particles, conventional casting techniques are not an appropriate fabrication technique for this kind of composite. Thus, other manufacturing routes such as powder metallurgy techniques have been developed to produce the copper-based composites [12]. The main areas of interest for copper and its composites are in the electronic packaging and heat sink industries, as well as for structural and frictional applications [12–14]. It should be noted that the electrical properties of copper composites can be seriously affected by impurities: some of them may precipitate during the heat treatment, and these precipitates deteriorate the electrical conductivity [13]. For instance, Caron et al. have reported that the electrical conductivity of copper can be lowered to only 86% IACS (International Annealed Copper Standard) as a consequence of 0.023% Fe addition during the fabrication process [13]. Moreover, it is reported that the presence of 0.3% Zr, 1.25% Al, or 0.1% P can lower the electrical conductivity of copper to 85%, 70%, or 50% IACS, respectively [12].

On the other hand, graphene nanoplatelets, due to their unique characteristics such as very high thermal conductivity (≈5000 W/(m·K)) and very low coefficient of thermal expansion in the in-plane direction (-1×10^{-6} K^{-1}), could attract considerable attention for use as reinforcing materials [15–18].

The main aim of this study is not only to investigate the effect of graphene nanoplatelets on the physical and mechanical characteristics of copper composites, but also to develop new Cu/GNP composite materials with improved mechanical strength, appropriate thermal and electrical conductivity, and tailored CTE.

2. Materials and Methods

2.1. Starting Materials

The starting materials which were used to produce the copper matrix nanocomposites with differing graphene nanoplatelet content included:

- Copper (Cu) powder, with 150–240 μm size and 99.5% purity (Figure 1a). This powder has an irregular morphology with a porous surface (spongy structure) and was supplied by Alfa Aesar, Ward Hill, MA, USA.
- Graphene nanoplatelets (GNPs) with 99% purity, ~100 nm thickness, 25 μm width, and surface area of 700 m^2/g, supplied by abcr GmbH, Karlsruhe, Germany (Figure 1b).

The densities of the copper powder and graphene nanoplatelets (GNPs) were 8.96 g/cm^3 and 2.2 g/cm^3, respectively.

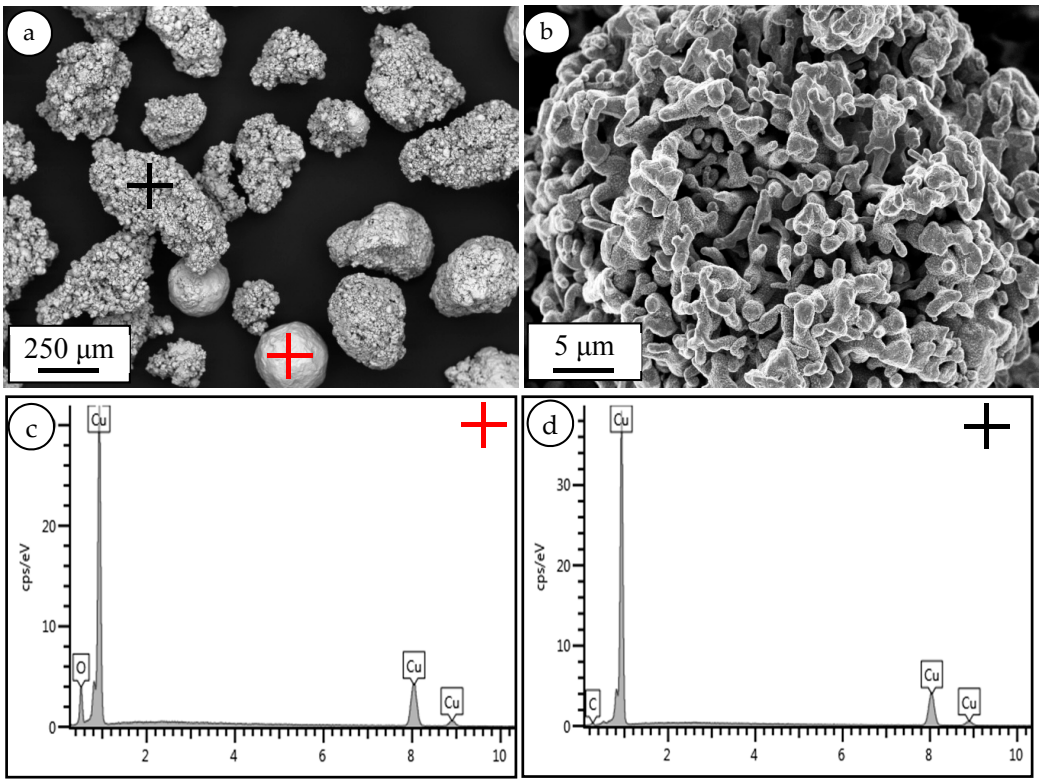

Figure 1. (**a**,**b**) SEM images of pure Cu powder with (**c**,**d**) the corresponding EDS analysis; the red cross and black cross belong to the copper oxide and copper particle, respectively.

2.2. Mixing

In principle, in order to take the advantage of the unique mechanical, thermal, and electrical properties of graphene nanoplatelets, it is necessary to achieve a uniform dispersion of GNPs within the metallic matrix. Therefore, in this work, the distribution of GNPs within the metal matrix was performed by means of mechanical milling and a novel wet mixing method proposed by Rashad et al. [19]; these techniques are described in the following sections.

2.2.1. Ball Milling

The nanocomposite powder preparation was carried out by a mechanical milling technique in a Pulverisette 5 planetary ball mill. The mixing of the starting powder was conducted in a hardened steel jar, and the milling media were 5 mm hardened stainless steel balls. The ball-to-powder ratio (BPR) was chosen to be equal to 10:1. During the milling process, methanol was used as a process control agent (PCA) to prevent the excessive cold welding of metallic powders, and an argon atmosphere was chosen in order to avoid oxidation during the milling. Mechanical milling was carried out by the agitation of a ball mill at a rotating speed of 200 rpm for 90 min, using a 30 min stop step after every 30 min of agitation in order to control the temperature during the milling. Reference samples of pure copper were mechanically milled under the same condition.

2.2.2. Wet Mixing

In this method, at first, graphene nanoplatelets and copper powders were separately dispersed in ethanol by means of ultrasonication. After ultrasonication for 45 min, the graphene nanoplatelet (GNP) suspension was added dropwise into the copper powder slurry to achieve the final content of GNPs. By adjusting the GNP content, composite powders with 4.0 vol % and 8.0 vol % graphene were

produced. The mixture was ultrasonicated for 60 min to obtain a homogeneous dispersion. Afterwards, the mixture was filtered and dried at 80 °C for 6 h to achieve the final nanocomposite powder.

2.3. Consolidation and Sintering

Die compaction of the powders is an economical and highly productive technique for fabricating the metal matrix nanocomposites [20]. Thus, as-prepared nanocomposite powders were compacted in a stainless steel die with 30 mm diameter at room temperature. The green cylindrical samples of Cu/GNP nanocomposites were sintered at 950 °C for 2 h under an inert atmosphere (N2). The corresponding bulk Cu/GNP composites were denoted as Cu–4.0 vol % GNPs and Cu–8.0 vol % GNPs, respectively.

2.4. Characterization

The morphology and microstructure of the starting and nanocomposite materials were characterized by means of a field-emission scanning electron microscope (FESEM; Merlin-Zeiss, München, Germany, operating at 15 kV) equipped with an energy-dispersive X-ray spectrometer (EDS). The theoretical densities of composites were calculated according to the rule of mixtures, whereas their relative densities were measured using the Archimedes method. X-ray diffraction (XRD) analysis of the nanocomposite was performed on a Philips X'Pert diffractometer using Cu Kα radiation, a tube voltage of 40 kV, and a tube current of 40 mA. In this research, Raman spectroscopy was used to evaluate the graphene structure during the fabrication process. Hence, the Raman spectra of graphene were obtained by using a Renishaw InVia Reflex micro-Raman spectrometer (Renishaw plc, Wotton-under-Edge, UK) equipped with a cooled charge-coupled device camera. The laser beam (λ = 514.5 nm) was focused using a 50$\times$ objective lens before irradiating the samples. In order to avoid damage to the samples, the integration time was 50 s and the laser power was reduced to 5 mW. The hardness measurement was performed by a Vickers hardness tester at a load of 5 kg for 15 s on a polished surface. The hardness values are the average of five different measurements on the same surface. Thermal expansion measurements were carried out by means of a SETSYS Evolution TMA with a heating rate of 5 °C/min. These measurements were carried out in the temperature range of 25–750 °C with a heating rate of 5° C/min in an argon atmosphere. The linear CTE was measured according to the following equation:

$$\alpha = \varepsilon \frac{1}{\Delta T} = \frac{\Delta L}{L_0} \frac{1}{\Delta T} \quad (1)$$

where, α is the CTE, ΔT is the temperature interval (T-298), L_0 is the starting length of the specimen, $\Delta L = L - L_0$ and $\varepsilon = \Delta L / L_0$. Cylindrical samples with a dimension of ϕ 5 mm $\times$ 120 mm were produced directly by means of a conventional powder metallurgy technique. Before starting the measurements, the TMA apparatus was calibrated according to DIN 51045 with NBS-Pt.

The elastic modulus of the composites was determined through a nondestructive test based on the impulse excitation vibration method. The reported results for the Young's modulus are the average of three different measurements. A laser-flash method was used to measure the thermal diffusivity, using a FLASHLINETM apparatus (Anter Corporation, Pittsburgh, PA, USA). The thermal conductivity of specimens was measured at 30 °C. In order to evaluate the electrical conductivity, firstly, the electrical resistivity of samples was measured; then, the electrical conductivity of specimens was calculated by using the inverse relationship of electrical resistivity and conductivity.

3. Results and Discussion

Figure 1 illustrates a representative FESEM image of pure copper powder used in this work; it can be seen that the copper particles have an irregular morphology with a porous structure. Moreover, in the copper starting powder, some dense particles (brighter particles) were revealed. According to the EDS analysis (red cross), they turned out to be copper oxide.

Figure 2a shows the FESEM images of the as-received GNPs. As can be seen in this image, the lateral size and thickness of the GNPs were approximately 25 μm and 100 nm, respectively. Figure 2b shows the Raman spectrum of the as-received graphene nanoplatelets. It can be seen that three main bands, corresponding to the D, G (+D'), and 2D vibrational modes, are present in the spectrum.

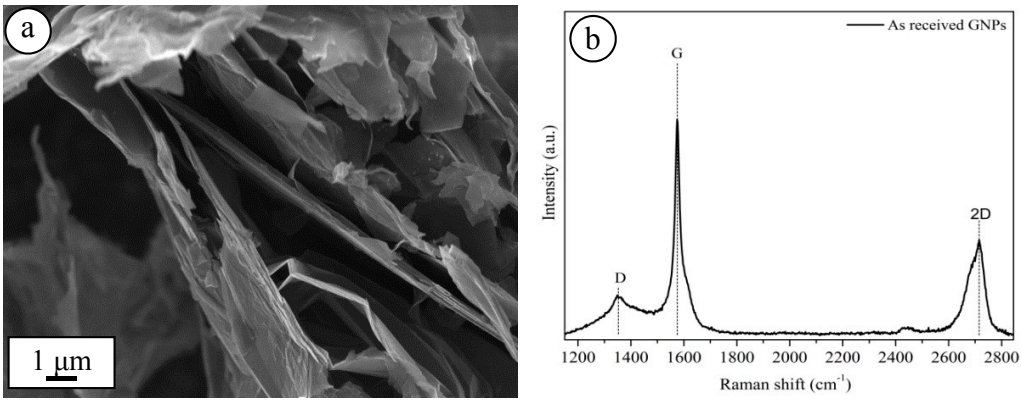

Figure 2. (**a**) SEM image and (**b**) Raman spectrum of as-received graphene nanoplatelets (GNPs).

In principle, the Raman spectrum of graphene-based material shows several bands in the range of 1200–2800 cm^{-1}. The first peak (D-band) at ~1350 cm^{-1} is due to a second-order scattering process which involves a graphene defect and a phonon. The second band at ~1580 cm^{-1} (G-band) is related to the E2g phonon at the center of the Brillouin zone [21]. The last important vibrational fingerprint deals with the 2D-band, also defined as the G'-band, which is spectrally located at ~2695 cm^{-1} for single-layer graphene [22].

According to the previous research, mixing a metal matrix with reinforcement by means of ball milling is the simplest and most common way [23–25]. Even if this technique shows great potential in the dispersion of ceramic particles within the metallic matrix, the following results provided some proof that advise against the ball milling technique as a dispersion method in the Cu/GNP nanocomposites. The Raman data, such as I_D/I_G and I_{2D}/I_G for as-received graphene and graphene in the composites after ball milling and wet mixing, are presented in Table 1.

Table 1. Raman data of as-received GNPs and Cu/GNPs after wet mixing and ball milling.

Composition	Ball Milled		Wet Mixed	
	I_D/I_G	I_{2D}/I_G	I_D/I_G	I_{2D}/I_G
As-received GNPs	0.112	0.511	0.112	0.511
Cu–8 vol % GNPs	0.893	0.584	0.127	0.525

The increase of I_D/I_G ratio signifies the introduction of defects into the carbon lattice as well as the reduction of the crystal size of the graphene platelets. Here, it is evident that these two undesirable phenomena have taken place during the ball milling and, accordingly, it was not possible to take advantage of the superior properties of graphene within the matrix. Surprisingly, the I_{2D}/I_G ratio did not change significantly; this means that the number of layers in the graphene did not change. It can be thus inferred that, after ball milling, the graphene was still multilayer. On the contrary, the I_D/I_G ratio of GNPs after wet mixing did not alter with respect to the as-received ones, implying that wet mixing could be a safe method to disperse the GNPs within the copper matrix.

Apart from the structural investigations by Raman spectroscopy, the morphology of the powder and the dispersion of graphene within the copper matrix were studied by means of a field-emission scanning electron microscope (FESEM). As can be seen in Figure 3, the distribution of the GNPs within

Cu–8 vol % GNPs nanocomposite powder was comparatively homogeneous. Moreover, it is evident that the graphene nanoplatelets were located in the open porosities on the copper particles and that most of the porosities on the surface of the copper particles were filled by GNPs.

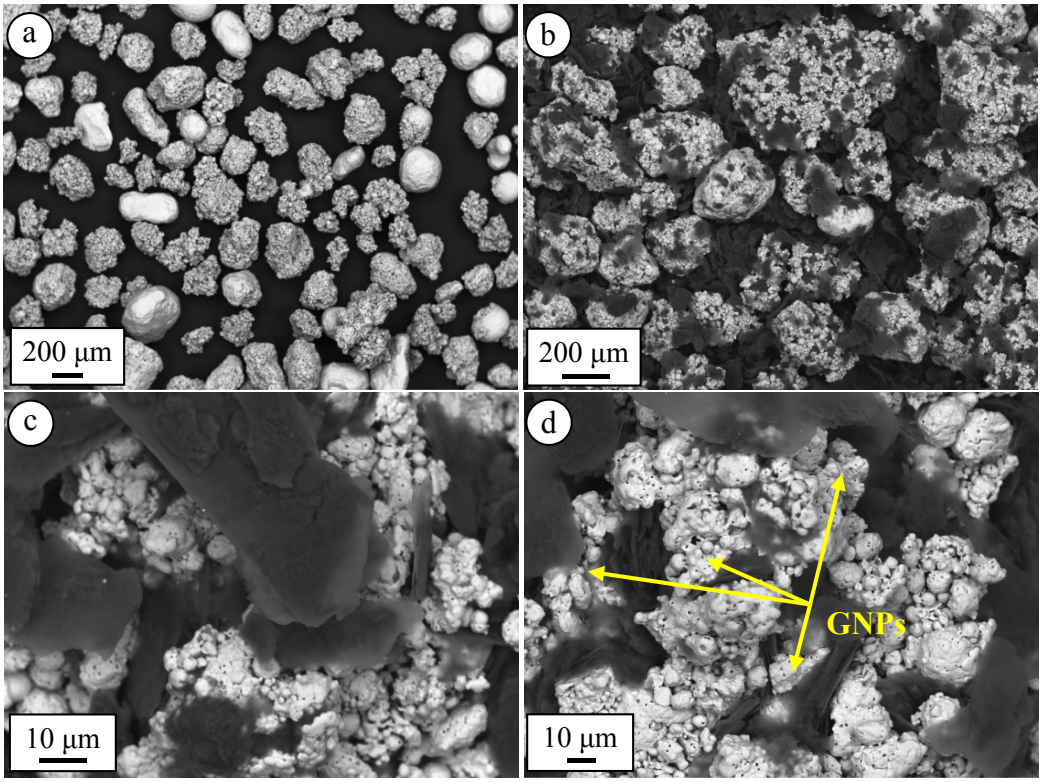

Figure 3. SEM images of (**a**) pure Cu and (**b**–**d**) Cu–8 Vol % GNPs composite powder mixture.

It is, therefore, likely that such a connection exists between the mixing technique and dispersion of GNPs as well as the properties of graphene after the mixing. It can be thus concluded that, through wet mixing, not only can a uniform dispersion be achieved but also the structure of the graphene can remain unchanged with respect to the starting graphene.

Figure 4a,b shows the microstructure of Cu–4.0 vol % GNPs and Cu–8.0 vol % GNPs, respectively, parallel to the compacting direction. According to these images, the dispersion of graphene seems to be homogeneous after the compaction and sintering process. However, it appears that, by increasing the graphene content up to 8 vol % GNPs (apart from the locating of graphene at the grain boundaries), the graphene platelets tend to form clusters and the number of agglomerates increases noticeably (red dashed circles). The average grain sizes of pure copper and composite were calculated based on the intercept method, and the results show that the addition of GNPs results in the reduction of grain size from 14 µm to 10 µm and 8 µm for Cu–4 vol % GNPs and Cu–8 vol % GNPs, respectively. The morphology of Cu–8.0 vol % GNPs perpendicular to the compacting direction is shown in Figure 4c. As can be seen, the graphene nanoplatelets are oriented mainly perpendicular to the compacting direction and this can result in anisotropic properties in the composite.

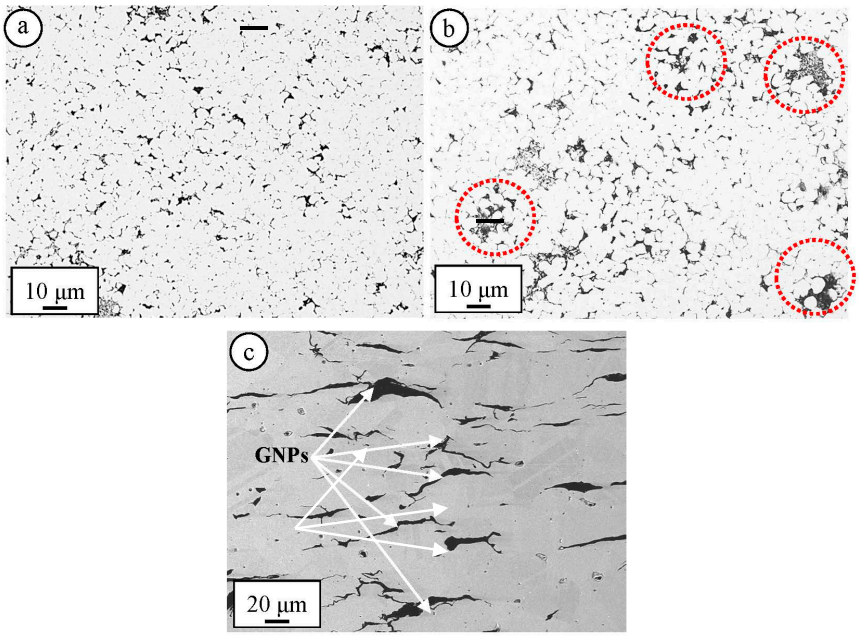

Figure 4. SEM images of sintered (**a**) Cu–4 vol % GNPs, (**b**) Cu–8 vol % GNPs parallel to the compaction direction, and (**c**) Cu–8 vol % GNPs perpendicular to the compaction direction.

The X-ray diffraction pattern of the Cu–8.0 vol % GNPs bulk sample after sintering at 950 °C for 2.5 h is presented in Figure 5. This pattern displays three clear peaks of copper ((111), (200), (220)) and an obvious peak of copper oxide, which provides further evidence of the presence of copper oxide in the starting copper powder. Furthermore, as can be seen in the XRD spectra, the peak at the 2θ value of 26.4° corresponds to the reflection of the graphitic structure (002). In the end, according to the XRD pattern, it could be deduced that no new phase was formed during the fabrication process.

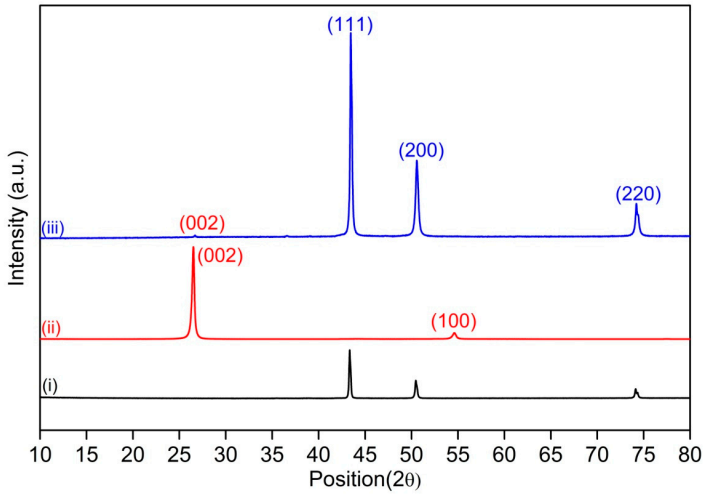

Figure 5. X-ray diffraction pattern of (i) pure copper, (ii) as-received GNPs, and (iii) Cu–8 vol % GNPs after sintering at 950 °C for 2.5 h.

Figure 6 illustrates the relative density and Vickers hardness of the copper nanocomposites as a function of graphene content. As can be seen, the relative density of copper and its composites decreased as a function of GNP content, particularly in the Cu–8 vol % GNPs sample. Thus, it is possible to conclude that the GNP content has a negative influence on the final density of composites. The decrease in the density of the composites was more pronounced than the theoretical value;

this discrepancy is probably due to the presence of extra porosity inside the composite. As shown earlier, GNPs tend to aggregate at higher content and result in the formation of steric obstacles in consolidation of the composites, restricting matrix material flow into the agglomerates [26].

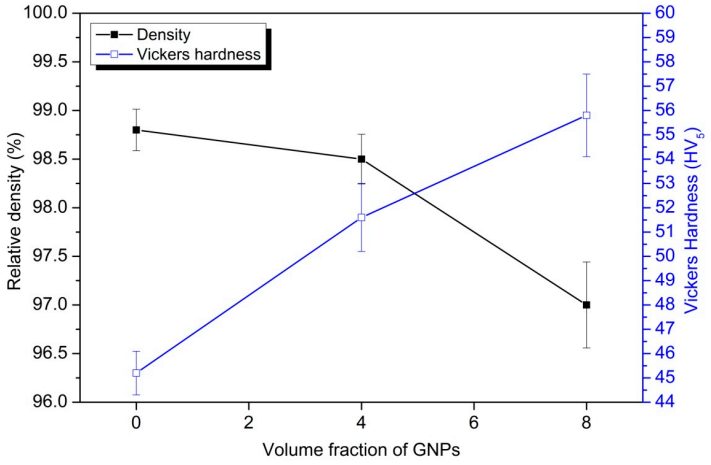

Figure 6. Vickers hardness and relative density of copper composites as a function of GNPs.

On the other hand, by increasing the GNP content, the Vickers hardness of the composites mainly increased, owing to the grain refinement effect of GNPs within the matrix.

The coefficient of thermal expansion values show the level of mismatch strains introduced into the matrix, either as a consequence of reinforcement addition with different properties or due to microstructural changes [27,28]. In fact, the grains of each phase have their physical properties, shapes, or volumes, leading to the residual stresses at the boundaries after thermal treatment [27,29]. These residual stresses at the boundaries can be transmitted without expansion of copper or debonding of the boundaries [30]. In this work, two different volume fractions of graphene were used as reinforcement in order to improve the mechanical properties and reduce the CTE of the copper composite. As shown previously, GNPs tend to orient preferentially perpendicular to the compacting direction, which leads to anisotropic properties. Due to a significant difference between the CTEs of graphene in the out-of-plane ($26 \times 10^{-6}/^{\circ}C$) and in-plane ($1.0 \times 10^{-6}/^{\circ}C$) directions, the anisotropic behavior in CTE of the composite was predictable. In the current research, all the CTE measurements for the Cu/GNP composite were carried out in the direction parallel to the compaction force.

As can be observed in Figure 7, the coefficient of thermal expansion of copper composites was decreased by increasing the GNP content. This phenomenon could be related to the more effective drag force on the grain boundary motion applied by GNPs. Moreover, GNPs exerted a higher compression force on the grain boundaries during the expansion of copper as a consequence of their very low CTE. This force during the expansion can limit this feature of copper grains, and resulted in the decrease in the CTE of the composites. Moreover, the measured CTEs in this work were in good agreement with those reported in the literature [31]. According to the existing literature on the CTE of composite materials, there are a number of available models to estimate the CTE of the composites [32–34]. As described earlier, the uniaxial compaction technique was used to fabricate the composites and, during the compaction, GNPs show a preferred orientation with respect to the compaction direction. Therefore, this kind of preferred orientation may affect the properties of composite materials in different axes and, thus, it should be taken into account for the modeling. This anisotropy property of the composite was considered by a simple model which was proposed by Schapery [35].

$$\alpha = \frac{\alpha_i E_i V_i + \alpha_o E_o V_o + \alpha_{Cu} E_{Cu} V_{Cu}}{E_i V_i + E_o V_o + E_{Cu} V_{Cu}} \quad (2)$$

Here, α is the coefficient of thermal expansion, E is the Young's modulus, and V is the volume fraction. The subscripts "i" and "o" represent the in-plane and out-of-plane properties of graphene, whereas the "Cu" subscript denotes the properties of copper.

As shown earlier, by increasing the GNPs content from 4.0 vol % to 8.0 vol %, the graphene started to agglomerate, and these clusters resulted in the lower interface area. Moreover, these agglomerates can affect the CTE of composites owing to either the anisotropic properties of graphene or the introduction of internal porosity. Substantially, due to the anisotropy of graphene, the whole volume of graphene can be sorted in two parts: one part with the positive contribution of graphene in overall CTE which is attributed to the Cu/GNP interface, and another one with a negative contribution of graphene in the CTE of the composite. Therefore, it can be defined that $V_j = c_i V_G$ (j = i and o) and c_a and c_c are the fractions of graphene volume which play the negative and positive roles in the final CTE. However, it should be mentioned that $c_i + c_o = 1$ and $V_i + V_o = V_G$. These are the main assumptions used in this model, and by inserting these assumptions in the previous equation the model could be as follows [8]:

$$\alpha = \frac{(\alpha_i E_i V_i + \alpha_o E_o (1 - c_i)) V_G + \alpha_{Cu} E_{Cu} V_{Cu}}{(E_i c_i + E_o (1 - c_i) V_G + E_{Cu} V_{Cu}}. \quad (3)$$

The parameters, such as the CTE of graphene in two directions and its mechanical properties, together with the data of copper used in this model, are presented in Table 2. However, the elastic modulus of copper was considered according to our experimental measurements.

Table 2. Parameters used in this model [8].

α_i (10^{-6} K^{-1})	α_o (10^{-6} K^{-1})	E_i (GPa)	E_o (GPa)	E_{Cu} (GPa)	α_{Cu} (10^{-6} K^{-1})
−1	26	1000	20	75	17.1

In order to have insight into the contribution of GNPs with a negative CTE to the thermal expansion of the composite, different volume fractions of graphene in the range of 4.0–8.0 were considered.

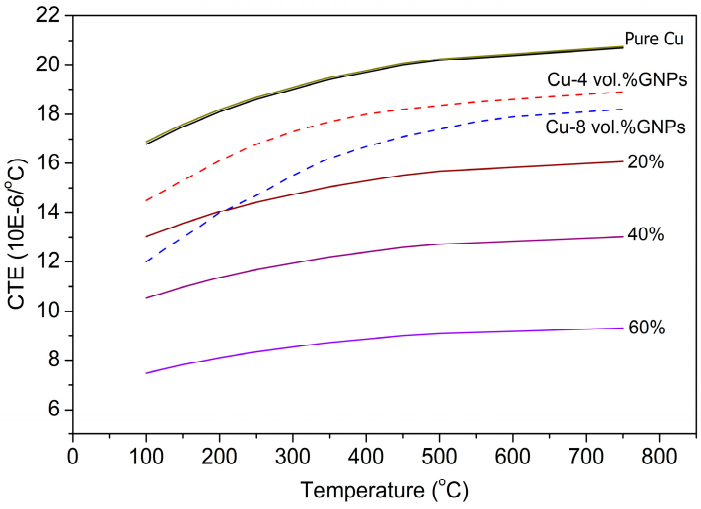

Figure 7. The theoretical predictions and experimental coefficient of thermal expansion of pure copper, Cu–4 vol % GNPs, and Cu–8 vol % GNPs as a function of temperature.

The measured CTEs of pure Cu, Cu–4.0 vol % GNPs, and Cu–8.0 vol % GNPs (dashed lines), together with the calculated CTEs at different volume fractions of graphene with negative CTE, are shown in Figure 7. The volume fraction of graphene with negative CTE can also be defined as the volume fraction of GNPs which are aligned perpendicular to the compaction. As can be seen

in Figure 7, if 60% of GNPs are oriented perpendicular to the compaction force, the effect of GNPs with a negative CTE would be significant; this effect changes as a function of the volume percentage of GNPs in this direction. By comparison with the measured CTE results of Cu–4.0 vol % GNPs and Cu–8.0 vol % GNPs, it seems that a less than 20% volume percentage of GNPs were aligned perpendicular to the compaction force. Nonetheless, it could conceivably be hypothesized that, if there were strong bonding between the Cu and GNPs, the CTE of the composite would be lower. Conversely, a lower efficiency of GNPs in terms of CTE reduction was found in Cu–8.0 vol % GNPs with respect to the Cu–4.0 vol % GNPs. This low efficiency could be attributed to the aggregation of GNPs at higher graphene content, poor interfacial bonding, and porosity.

Figure 8 compares the experimental data and theoretical calculations of the Young's modulus of Cu/GNPs composites as a function of GNP content. Previous research has established several models in order to predict the effect of reinforcement addition on the elastic behavior of MMNCs. Halpin and Tsai proposed a model considering the distribution and aspect ratio of reinforcement as the main assumptions; the model can be expressed as follows [36]:

$$E_c = E_m\left[\frac{3}{8}\times\frac{1+2/3\eta_L pV_G}{1-\eta_L V_r}+\frac{5}{8}\times\frac{1+2\eta_T V_G}{1-\eta_T V_r}\right], \quad (4)$$

$$E_{||} = E_m\left[\frac{1+2/3\eta_L pV_G}{1-\eta_L V_G}\right], \quad (5)$$

$$\eta_L = \frac{E_G/E_m-1}{E_G/E_m+2/3p}, \quad (6)$$

$$\eta_T = \frac{E_G/E_m-1}{E_G/E_m+2}, \quad (7)$$

where E is the elastic modulus, V is the volume fraction, and p is the aspect ratio of graphene. The subscripts "c", "G", and "m" denote the composite, graphene, and matrix. This model considers the random distribution and preferred orientations of GNPs within the matrix. It would be possible to predict this anisotropic effect by Equations (4) and (5) for random distribution (E_c) and preferred orientation ($E||$). The aspect ratio of the GNPs is calculated by dividing the length of graphene by its thickness. In the calculations, the elastic modulus of Cu was considered to be 75 GPa (according to our measurement), and the elastic modulus of graphene was 1.0 TPa (reported from the previous works [37]). The lower Young's modulus of copper with respect to the theoretical value can be related to the purity of the starting powder and the porosity content of sintered specimens. As can be seen in Figure 8, the elastic properties of the composite can be improved through graphene addition, but it is clear that the practical improvement is lower than the predictions. This discrepancy suggests that the elastic properties of the composite could be improved more through the improvement of the process parameters and quality of graphene. This difference between the models and practical data could be attributed to the following reasons: (i) since as-received graphene used in this research is not a defect-free graphene, its real elastic modulus might be lower than the theoretical one, (ii) poor interfacial bonding between Cu and GNPs, and (iii) random distribution of graphene with various orientations could disturb the unidirectional load-transfer mechanism and reduce the composite properties. These findings clearly imply that the dispersion of graphene at higher content is a key challenge. Furthermore, this comparison shows that further improvement in the mechanical properties can be achieved through either the optimization of the process parameters or by using some post-processing steps.

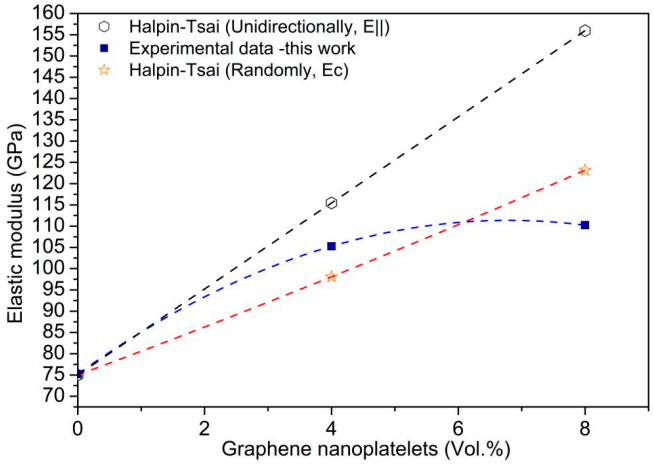

Figure 8. Comparison between the measured CTE and theoretical calculations of elastic modulus (Ec and E||) of Cu/GNPs composites as a function of GNP content.

Table 3 shows the characteristics of some metals and alloys which are used in electronic packaging, together with the experimental results which were achieved in this research. As can be seen in this table, in spite of the proper thermal expansion of Cu–Mo and Cu–W at ambient temperatures, the medium thermal conductivity and high density of these two materials limits their application as electronic packaging materials. In the case of Cu–Ni–Sn, although the electrical resistivity of this alloy is increased with respect to pure copper, its thermal conductivity is significantly decreased, and the thermal expansion of this alloy is still high. These characteristics either limit its application or reduce its heat dissipation efficiency. As can be seen in Table 3, the thermal and electrical conductivity of copper composites were decreased by increasing the GNP content. These reductions in thermal and electrical conductivities, which are affected significantly by activities of free electrons, can be related to several reasons. In this work, poor interfacial bonding (interfacial porosity) and grain refinement can be considered as two main sources of these reductions. However, Chen et al. have reported that the high O content produced in the PM (Powder Metallurgy) process can be another reason [38,39]. It can be thus concluded that grain refinement, high oxygen content interface, and porosity within the matrix increase electron scattering and consequently decrease electron and thermal conductivities. In comparison with these commonly used materials in heat sink applications, the high thermal conductivity and low thermal expansion of Cu/GNP composites, which were developed within this work, make them interesting materials for use in the electronic packaging industry.

Table 3. Typical properties of some metallic materials used in electronic packaging.

Metals and Alloys	Thermal Conductivity at 0–100 °C (W/m·K)	Electrical Resistivity at 20 °C (Ω m × 10^8)	Thermal Expansion (1/k × 10^6)	Density at 20 °C (g/cm^3)	Reference
Aluminium (Al)	238	2.8	23.5	2.7	[9]
Cu–Ni–Sn	50	14	17.1	8.88	[9]
Copper (Cu)	393	1.7	17	8.9	[40]
Red Brass (15% Zn)	151	4.66	18.7	8.8	[40]
CuW	180–220	–	7–9	>9	[40]
CuMo	160–185	–	7–9	9	[41]
Copper (Cu)	350	1.45	18	8.9	Current work
Cu–4 vol % GNPs	304	1.49	14	8.7	Current work
Cu–8 vol % GNPs	262	1.55	12	8.3	Current work

4. Conclusions

The Cu/GNP nanocomposites were successfully fabricated by wet mixing followed by a classical powder metallurgy route. Raman analysis of the GNPs and microstructural observations confirm that ball milling is not an appropriate technique to disperse the GNPs within the copper matrix, whereas the wet mixing method has great potential to be used as a dispersion technique. Through wet mixing, the graphene nanoplatelets were randomly distributed within the matrix and most of the graphene was located at the copper grain boundaries, thus leading to grain refinement. During the compaction of the composite powder, the graphene nanoplatelets oriented preferentially perpendicular to the compaction direction, which implies that the produced composite might show anisotropic properties. By increasing the graphene content up to 8 vol %, apart from the locating of graphene at the grain boundaries, the nanoplatelets tend to form clusters and the number of agglomerates increases noticeably. By increasing the graphene content, the Vickers hardness of the composites increased as well as their elastic modulus, mainly owing to the grain refinement effect. The variation in the coefficient of thermal expansion of copper composites at different temperatures from 100 °C to 750 °C showed that the coefficient of thermal expansion of copper composites decreased by increasing the GNP content. On the other hand, it is found that the combination of grain refinement and porosity content were responsible for decreased electron and thermal conductivities. In addition, it was found that, through the addition of GNPs, it would be possible to produce a novel composite with almost high thermal and electrical conductivity together with low thermal expansion and density. Since the achieved results are desirable characteristics for the electronic packaging industry, this fabricated composite is one of the most interesting candidates for use in heat sink applications. All in all, it can be concluded that the fabrication of composites reinforced by GNPs faces several challenges, such as the dispersion of graphene at higher content levels, interfacial bonding between the copper and GNPs, and the preferred orientation of graphene during the fabrication process.

Author Contributions: In this work, Abdollah Saboori and Seyed Kiomars Moheimani conceived and designed the experiments and thereafter performed the experiments. Abdollah Saboori and Matteo Pavese analyzed the data. Claudio Badini and Paolo Fino contributed reagents, materials, and analysis tools. Abdollah Saboori wrote the paper and the other authors revised the paper.

Conflicts of Interest: The authors declare no conflict of interest.

References

1. Macke, A.; Schultz, B.F. Metal matrix composites offer the automotive industry and opportunity to reduce vehicle weight, improve performance. *Adv. Mater. Process.* **2012**, *170*, 19–23.
2. Deng, C.F.; Ma, Y.X.; Zhang, P.; Zhang, X.X.; Wang, D.Z. Thermal expansion behaviors of aluminum composite reinforced with carbon nanotubes. *Mater. Lett.* **2008**, *62*, 2301–2303. [CrossRef]
3. Chen, Y.; Zhang, X.; Liu, E.; He, C.; Han, Y.; Li, Q.; Nash, P.; Zhao, N. Fabrication of three-dimensional graphene/Cu composite by in-situ CVD and its strengthening mechanism. *J. Alloys Compd.* **2016**, *688*, 69–76. [CrossRef]
4. Saboori, A.; Pavese, M.; Badini, C.; Fino, P. A Novel approach to enhance the mechanical strength and electrical and thermal conductivity of Cu-GNP nanocomposites. *Metall. Mater. Trans. A* **2017**, 1–13. [CrossRef]
5. Du, H.; Lu, D.; Qi, J.; Shen, Y.; Yin, L.; Wang, Y.; Zheng, Z.; Xiong, T. Heat dissipation performance of porous copper with elongated cylindrical pores. *J. Mater. Sci. Technol.* **2014**, *30*, 934–938. [CrossRef]
6. Memis, I. Electronic Packaging Materials: Properties and Selection. In *Reference Module in Materials Science and Materials Engineering*; Elsevier B.V.: Amesterdam, The Netherlands, 2016, ISBN 978-0-12-803581-8.
7. Huang, D.-S.; Tu, W.-B.; Zhang, X.-M.; Tsai, L.-T.; Wu, T.-Y.; Lin, M.-T. Using Taguchi method to obtain the optimal design of heat dissipation mechanism for electronic component packaging. *Microelectron. Reliab.* **2016**, *65*, 131–141. [CrossRef]
8. Kováčik, J.; Emmer, Š. Thermal expansion of Cu/graphite composites: Effect of copper coating. *Kov. Mater.* **2011**, *49*, 411–416.

9. WC, F. *Materials in Electronic Packaging, Hand Book of Materials Selection*; Kutz, M., Ed.; John Wiley & Sons Inc.: New York, NY, USA, 2002.
10. Chen, B.; Bi, Q.; Yang, J.; Xia, Y.; Hao, J. Tribology international tribological properties of solid lubricants (graphite, h-BN) for Cu-based P/M friction composites. *Tribol. Int.* **2008**, *41*, 1145–1152. [CrossRef]
11. Hanada, K.; Matsuzaki, K.; Sano, T. Thermal properties of diamond particle-dispersed Cu composites. *J. Mater. Process. Technol.* **2004**, *153–154*, 514–518. [CrossRef]
12. Davis, J.R. *Powder Metallurgy: Copper and Copper Alloys. ASM Specialty Handbook*; ASM International: Geauga County, OH, USA, 2001, ISBN 0-87170-726-8.
13. Caron, R.N. *Copper Alloys: Properties and Applications*, 2nd ed.; Elsevier B.V.: Amesterdam, The Netherlands, 2001.
14. Kundig, K.J.A.; Cowie, J.G. *Mechanical Engineers' Handbook: Materials and Mechanical Design*, 3rd ed.; Kutz, M., Ed.; John Wiley & Sons, Inc.: New York, NY, USA, 2006, ISBN 9780471449904.
15. Rashad, M.; Pan, F.; Asif, M.; Tang, A. Powder metallurgy of Mg–1%Al–1%Sn alloy reinforced with low content of graphene nanoplatelets (GNPs). *J. Ind. Eng. Chem.* **2014**, *20*, 4250–4255. [CrossRef]
16. Liu, L.; Qing, M.; Wang, Y.; Chen, S. Defects in graphene: Generation, healing, and their effects on the properties of graphene: A review. *J. Mater. Sci. Technol.* **2015**, *31*, 599–606. [CrossRef]
17. Van Chuc, N.; Thanh, C.T.; Van Tu, N.; Phuong, V.T.Q.; Thang, P.V.; Thi, N.; Tam, T. A simple approach to the fabrication of graphene-carbon nanotube hybrid films on copper substrate by chemical vapor deposition. *J. Mater. Sci. Technol.* **2015**, *31*, 479–483. [CrossRef]
18. Saboori, A.; Pavese, M.; Badini, C.; Fino, P. Microstructure and thermal conductivity of Al-Graphene composites fabricated by powder metallurgy and hot rolling techniques. *Acta Metall. Sin. (Engl. Lett.)* **2017**, *30*, 675–687. [CrossRef]
19. Rashad, M.; Pan, F.; Tang, A.; Asif, M.; Hussain, S.; Gou, J.; Mao, J. Improved strength and ductility of magnesium with addition of aluminum and graphene nanoplatelets (Al + GNPs) using semi powder metallurgy method. *J. Ind. Eng. Chem.* **2015**, *23*, 243–250. [CrossRef]
20. Saboori, A.; Novara, C.; Pavese, M.; Badini, C.; Giorgis, F.; Fino, P. An investigation on the sinterability and the compaction behavior of aluminum/graphene nanoplatelets (GNPs) prepared by powder metallurgy. *J. Mater. Eng. Perform.* **2017**, *26*, 993–999. [CrossRef]
21. Ferrari, A.C.; Robertson, J. Resonant Raman spectroscopy of disordered, amorphous, and diamondlike carbon. *Phys. Rev. B* **2001**, *64*, 075414. [CrossRef]
22. Mohiuddin, T.M.G.; Lombardo, A.; Nair, R.R.; Bonetti, A.; Savini, G.; Jalil, R.; Bonini, N.; Basko, D.M.; Galiotis, C.; Marzari, N.; et al. Uniaxial strain in graphene by Raman spectroscopy: G peak splitting, Grüneisen parameters, and sample orientation. *Phys. Rev. B* **2009**, *79*, 205433. [CrossRef]
23. Perez-Bustamante, R.; Bolanos-Morales, D.; Bonilla-Maetinez, J.; Estrada-Guel, I. Microstructural and hardness behavior of graphene-nanoplatelets/aluminum composites synthesized by mechanical alloying. *J. Alloys Compd.* **2014**, *615*, S578–S582. [CrossRef]
24. Pérez-Bustamante, R.; Gómez-Esparza, C.D.; Estrada-Guel, I.; Miki-Yoshida, M.; Licea-Jiménez, L.; Pérez-García, S.A.; Martínez-Sánchez, R. Microstructural and mechanical characterization of Al–MWCNT composites produced by mechanical milling. *Mater. Sci. Eng. A* **2009**, *502*, 159–163. [CrossRef]
25. Tabandeh-khorshid, M.; Ferguson, J.B.; Schultz, B.F.; Kim, C.; Cho, K.; Rohatgi, P.K. Strengthening mechanisms of graphene- and Al_2O_3-reinforced aluminum nanocomposites synthesized by room temperature milling. *Mater. Des.* **2016**, *92*, 79–87. [CrossRef]
26. Chu, K.; Jia, C.C. Enhanced strength in bulk graphene-copper composite. *Phys. Status Solidi A* **2014**, *211*, 184–190. [CrossRef]
27. Levy-Tubiana, R.; Baczmanski, A.; Lodini, A. Relaxation of thermal mismatch stress due to plastic deformation in an Al/SiCp metal matrix composite. *Mater. Sci. Eng. A* **2003**, *341*, 74–86. [CrossRef]
28. Qian, L.H.; Wang, S.C.; Zhao, Y.H.; Lu, K. Microstrain effect on thermal properties of nanocrystalline Cu. *Acta Mater.* **2002**, *50*, 3425–3434. [CrossRef]
29. Kassner, M.E.; Hayes, T.A. Creep cavitation in metals. *Int. J. Plast.* **2003**, *19*, 1715–1748. [CrossRef]
30. Weidenmann, K.; Tavangar, R.; Weber, L. Mechanical behaviour of diamond reinforced metals. *Mater. Sci. Eng. A* **2009**, *523*, 226–234. [CrossRef]
31. Wang, X.; Li, J.; Wang, Y. Improved high temperature strength of copper-graphene composite material. *Mater. Lett.* **2016**, *181*, 309–312. [CrossRef]
32. Hale, D.K. The physical properties of composite materials. *J. Mater. Sci.* **1976**, *11*, 2105–2141. [CrossRef]

33. Turner, P.S. Thermal-expansion stresses in reinforced plastics. *J. Res. Natl. Bur. Stand.* **1946**, *37*, 239–250. [CrossRef]
34. Hashin, Z.; Shtrikman, S. A variational approach to the theory of the elastic behaviour of multiphase materials. *J. Mech. Phys. Solids* **1963**, *11*, 127–150. [CrossRef]
35. Schapery, R.A. Thermal expansion coefficients of composite materials based on energy principles. *J. Compos. Mater.* **1968**, *2*, 380–404. [CrossRef]
36. Saboori, A.; Pavese, M.; Badini, C.; Fino, P. Development of Al- and Cu-based nanocomposites reinforced by graphene nanoplatelets: Fabrication and characterization. *Front. Mater. Sci.* **2017**, *11*, 171–181. [CrossRef]
37. Lee, C.; Wei, X.; Kysar, J.W.; Hone, J. Measurement of the elastic properties and intrinsic strength of monolayer graphene. *Science* **2008**, *321*, 385–388. [CrossRef] [PubMed]
38. Chen, B.; Li, S.; Imai, H.; Jia, L.; Umeda, J.; Takahashi, M.; Kondoh, K. Carbon nanotube induced microstructural characteristics in powder metallurgy Al matrix composites and their effects on mechanical and conductive properties. *J. Alloys Compd.* **2015**, *651*, 608–615. [CrossRef]
39. Chen, B.; Jia, L.; Li, S.; Imai, H.; Takahashi, M.; Kondoh, K. In situ synthesized Al_4C_3 nanorods with excellent strengthening effect in aluminum matrix composites. *Adv. Eng. Mater.* **2014**, *16*, 972–975. [CrossRef]
40. Tong, X.C. Electronic Packaging Materials and Their Functions in Thermal Managements. In *Advanced Materials for Thermal Management of Electronic Packaging*; Springer: New York, NY, USA, 2011; pp. 131–167, ISBN 978-1-4419-7759-5.
41. Wilson, J. *Thermal Conductivity of Common Alloys in Electronics Packaging*; Electronics Cooling: Montgomery County, PA, USA, 2007.